Steel and Composite Structures, Vol. 1, No. 1 (2001) 75-96
DOI: http://dx.doi.org/10.12989/scs.2001.1.1.075

The ECBL approach for interactive buckling of thin-walled steel members

Dan Dubina†

Department of Steel Structures and Structural Mechanics, Civil Engineering and Architecture Faculty, "Politehnica" University of Timisoara, Stadion 1, RO-1900, Timisoara, Romania

Abstract. Actual buckling curves are always characterised by the erosion of ideal buckling curves. In case of compact sections this erosion is due to the imperfections, while for thin-walled members, a supplementary erosion is induced by the phenomenon of coupled instabilities. The ECBL approach-Erosion of Critical Bifurcation Load - represents a practical and convenient tool to characterise the instability behaviour of thin-walled members. The present state-of-art paper describes the theoretical background of this method and the applications to cold-formed steel sections in compression and bending. Special attention is paid to the evaluation methods of erosion coefficient and to their validation. The ECBL approach can be also used to the plastic-elastic interactive buckling of thin-walled members, and the paper provides significant results on this line.

Key words: thin-walled steel sections; local buckling; overall buckling; critical load; coupled instabilities; imperfections; erosion; coupling range; buckling curves; local plastic mechanism.

1. Introduction

The instability behaviour of bar members is generally characterised by stable post-critical modes. However the interaction of two stable symmetric post-critical modes may generate an unstable coupled asymmetric mode, rendering the member highly sensitive to imperfections. In such a case a significant erosion of critical load occurs. Examining the cases of coupled instability, we find that two very different types exist (Gioncu 1994):

(a) *naturally coupled instabilities*; which result in garland curves. Two forms of instability are possible in the intersection points of these curves. The post-critical curves can be stable for uncoupled modes, but by coupling, they become unstable. The phenomenon of buckling patterns change in plates and shells, due to this mode interaction, is well known, but, in some way, it may by found also in the case of thin-walled members (Fig. 1).

(b) *coupling due to design*; when the geometric dimensions of structure are chosen such as two or more buckling modes are simultaneously possible (Fig. 2). For this case, the optimisation based on the simultaneous mode design principle plays a very important role and the attitude of the designer in regard with this principle is decisive. This type of coupling is the most interesting in practice.

Another classification of coupled instabilities refers to the linearity or non-linearity of coupling:

(a) *linear coupling*; this occurs when two modes are coupling from the origin, independently of the presence of imperfections. An example is the interaction between flexural and torsional

†Professor

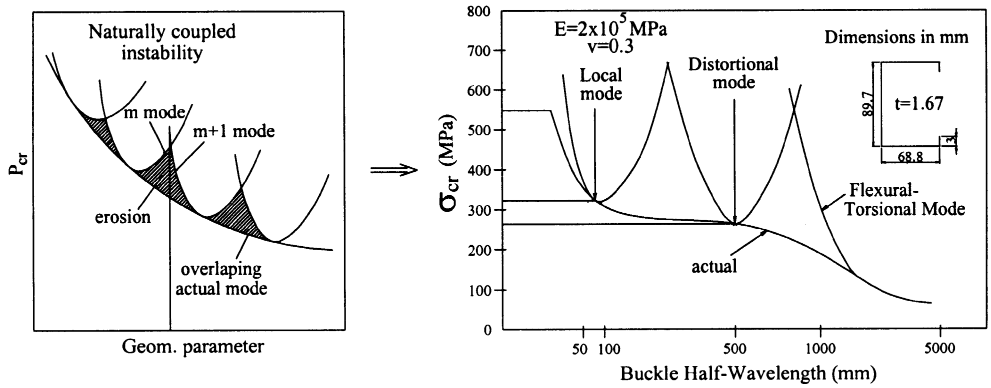

Fig. 1 Natural coupled instability: example for lipped channel section analysed with a spline finite strip buckling program (Lau and Hancock 1990)

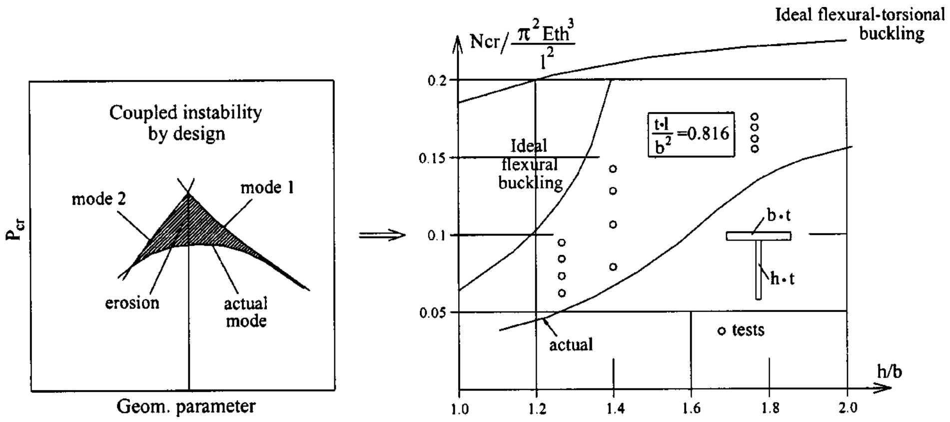

Fig. 2 Coupled instability by design: example for T section with test evidences (Gioncu 1992)

buckling of mono-symmetrical sections;

(b) *non-linear coupling*; this exist for some geometrical proportions of structures only, and the presence of the geometrical imperfections is necessary for coupling; this coupling doesn't exist for ideal structure. For instance, this is the case of the interaction between flexural buckling and torsional-flexural buckling of some mono-symmetrical cross-section (Fig. 2).

The general meaning of coupled instability phenomenon is related, in fact, to non-linear coupling. Due to the imperfections, an interaction erosion of critical bifurcation load occurs. This erosion is maximum in the coupling point vicinity. For bar members, an interactive slenderness range, in which sensitivity to imperfections is increased, may be identified. Classes of interaction types, separated by specific levels of erosion intensity, may be defined.

Given a compression member, we are assuming two simultaneous buckling modes may occur. If N_u is the critical ultimate load, and N_{cr} the ideal critical one, the following relation may be written:

$$N_u = (1-\psi)N_{cr} \tag{1}$$

The *erosion factor* ψ was introduced as a *measure* of erosion of critical load. Gioncu (1994) has classified the interaction types by means of this erosion factor, as follows:

class I: weak interaction (W), $\psi \le 0.1$;

class II: moderate interaction (M), $0.1 < \psi \le 0.3$;

class III: strong interaction (S), $0.3 < \psi \le 0.5$;

class IV: very strong interaction (VS), $\psi > 0.2$.

Obviously, an appropriate framing of each coupled instability into the relevant class is very important because the methods of analysis used for design have to be different from one class to another. In case of week or moderate interaction, structural reliability will be provided by simply using of design code safety coefficients, while in case of strong or very strong interaction, special methods are needed.

2. Interaction types in bar members (Dubina 1996)

As shown in Fig. 3 the buckling modes can be characterised by their wavelengths. If the two modes that couple have comparable wavelengths, then their unstable post-critical path shows a weak or moderate interaction; this is the case of interaction between flexural and flexural-torsional buckling in case of mono-symmetrical compression members.

If strong differences exist between the two modes, as in the case when overall and local modes couple, a moderate to strong interaction occurs; this is the case of laced built-up columns. Very different behaviour is resulting when multiple local buckling modes occur simultaneously under the same critical load. For a long bar, multiple load buckling modes with m-1, m, m+1 half-wavelength may interact in the first form of the interaction (Fig. 3) and lead to an unstable post-critical behaviour. It is very important to know that such interaction provides a *localisation of the buckling* patterns, because the localised mode has a more pronounced unstable slop than that periodical one. The second interaction is due to the interaction of the stable post-critical general buckling with an unstable post-critical localised buckling and yields to a very unstable post-critical behaviour. This interaction produces a great erosion of the critical load due to geometrical imperfection, and characterises the behaviour of thin-walled members.

If the localised mode occurs prior to the overall one, the member post-buckling behaviour may be modified by material yielding, and leads to a local plastic mechanism. In this case the interaction is

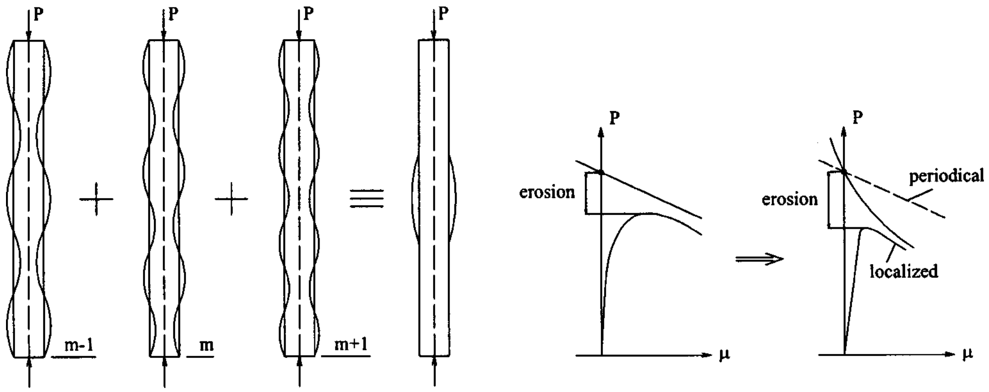

Fig. 3 Localised buckling pattern generated by multiple local buckling modes interaction

produced between the overall mode, which corresponds to an elastic non-linear behaviour of the member, and a local plastic collapse mechanism, associated with stub column behaviour. Murray and Khoo (1981) have described the theoretical background of this type of behaviour, and have given a method, which closely predicts the local plastic strength of thin-walled short members.

If the plastic mechanism is properly identified, the resistance of the short member, either in compression or bending, can be more appropriately evaluated, than using the “effective width” approach. The reason is that, even the local buckling firstly appears in case of short members, it always changes into local plastic mechanism when the member fails.

For stub columns the “*effective width*” approach operates with the plastic strength of the effective cross-section, while effective width of component walls is evaluated in terms of the elastic critical stress; this represents an important inconsistency of this theoretical model. The “*local plastic mechanism*” operates with the “*real*” plastic strength, assuming the thin-walled cold-formed stub column fails by forming plastic hinge and/or plastic zone, as effect of the localisation of buckling pattern. Consequently, the local-global interactive buckling could be regarded as one of *plastic-elastic* type, and not as an *elastic-elastic* one.

The columns of intermediate slenderness with open thin-walled section may also buckle in a distortional mode. If the local buckling mode keeps straight the wall junctions, the distortional mode, as shown in Fig. 4, involves rotations of the flange-lip about the flange-web junctions. This buckling mode has been referred as a local-torsional mode in some reports (Lau and Hancock 1988, Al-Bermani 1994). However the distorsion of cross-section may involves in some cases the web-flange junctions too.

Local buckling can occur either simultaneously with distortional buckling, or at higher or lower load. The question is, if the distortional mode cannot be regarded as a local mode and, consequently, due to interaction with other local modes, no localised buckling pattern occurs? The tests by Kwon and Hancock on lipped channel section (Hancock 1994) have demonstrated that no unstable post-critical path results in the local with distortional buckling interaction. Thus, the distortional buckling strength can be assessed independently of whether local buckling is occurring simultaneously.

In the case of thin-walled beams, when the elastic local buckling load of compression flange is close to the lateral-torsional buckling one, the actual strength may be reduced by imperfection effect. Some small reductions were reported in (Menken 1991) for thin flange beams in uniform bending, so even through local buckling will significantly reduce the resistance to flexural-torsional buckling, generally no strong interaction erosion occurs.

The situation is similar to the case of interaction between distortional and lateral-torsional buckling, even through the distortion of cross-section may involve an important reduction of

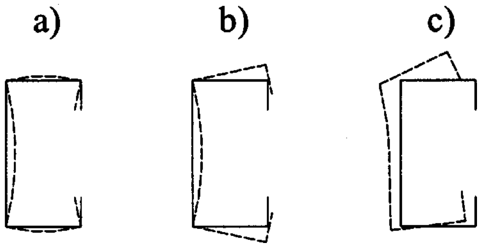

Fig. 4 Local and distortional buckling modes in a thin-walled lipped channel section: a) local; b) local-torsional; c) distortional

Table 1 Coupled instabilities in bar members

No.	Bar member type	Instability modes	Class of interaction
1.	Mono-symmetrical columns	F+FT=FFT	W to M $\psi = 0.3$
2.	Built-up columns	F+L=FL	M $0.1 < \psi = 0.3$
3.	Thin-walled columns	F+L=FL FT+L=FTL F+FT+L=FFTL	S to VS $\psi = 0.3$
		F+D=FD FT+D=FTD F+FT+D=FFTD	M to S $0.3 = \psi = 0.5$
4.	Thin-walled beams	LT+L=LTL LT+D=LTD	M $\psi = 0.3$

Legend: F=flexural buckling; FT=flexural-torsional buckling; L=local buckling; D=distortional buckling; W=week interaction; M=moderate interaction; S=strong interaction; VS=very strong interaction

member buckling resistance.

Table 1 summarises the main coupled instability cases, which may appear within the bar members.

3. ECBL approach-a way to adapt the Ayrton-Perry formula for interactive buckling of bar members

3.1. Ayrton-Perry formula for global buckling of compression member

Considering a pinned supported bar in compression, the Ayrton-Perry formula can be expressed in terms of axial force as follows:

$$(1 - \bar{N})(1 - \bar{\lambda}^2 \bar{N}) = \eta \bar{N} \tag{2}$$

with:

$\bar{N} = \dfrac{N}{N_{pl}}$, the dimensionless axial compression force,

$\bar{\lambda} = \sqrt{\dfrac{N_{pl}}{N_{cr}}}$, the reduced member slenderness,

and $N_{pl} = Af_y$, the plastic strength of full cross-section.

In order to generate the European buckling curves (Eurocode 3 1996), the following relation was proposed for the generalised imperfection factor η (Rondal and Maquoi 1979):

$$\eta = \alpha(\bar{\lambda} - 0.2) \tag{3}$$

which has to be replaced in Eq. (2). It gives:

$$(1 - \bar{N})(1 - \bar{\lambda}^2 \bar{N}) = \alpha(\bar{\lambda} - 0.2)\bar{N} \tag{4}$$

Solving this equation in terms of $\overline{N}$ it can be obtained

$$\overline{N}_{1.2} = \frac{1 + \alpha(\bar{\lambda} - 0.2) + \bar{\lambda}^2}{2\bar{\lambda}^2} \pm \frac{1}{2\bar{\lambda}^2}\sqrt{[1 + \eta(\bar{\lambda} - 0.2) + \bar{\lambda}^2]^2 - 4\bar{\lambda}^2} \tag{5}$$

in which only (-) is significant. The imperfection coefficient a was statistically calibrated via some representative series of experimental test results in order to define the five European buckling curves:

Curve	a_0	a	b	C	d
α	0.13	0.21	0.34	0.49	0.76

If the component walls of the member cross-section are prone to local buckling, according to Winter and Von Karman's theories, the yield stress, f_y yield stress is assumed to be distributed on the effective area of the cross-section only, i.e., A_{eff}:

$$A_{eff} = QA \tag{6}$$

where

$$Q = \frac{A_{eff}}{A} \tag{7}$$

where Q is the reducing factor of gross area which should be calculated on the basis of effective width principle.

The reduced cross-section plastic strength, in this case, will be:

$$N_{pl} = f_y A_{eff} = (f_y Q)A \tag{8}$$

and, as consequence, Eq. (2) becomes:

$$(Q - \overline{N})(1 - \bar{\lambda}^2\overline{N}) = \alpha(\bar{\lambda} - 0.2)\overline{N} \tag{9}$$

Eq. (9) represents the Ayrton-Perry formula for *Overall-Local Interactive Buckling*.

3.2. Erosion of the overall-local coupled buckling load

On the basis of Erosion of Critical Bifurcation Load (ECBL) theory (Dubina 1990, 1993, 1998), a new approach was proposed to evaluate the ultimate strength in overall-local interactive buckling. Assuming the two theoretical simple instability modes that couple in a thin-walled compression member, are the Euler bar instability mode, $\overline{N}_{\alpha} = 1/(\sqrt{\bar{\lambda}})$ and the local instability mode, $\overline{N}_L = Q$ (Fig. 5), then the maximum erosion of critical load, due both, to the imperfections and coupling effect occurs in the coupling point $\bar{\lambda}_C = 1/\sqrt{Q}$. The interactive buckling load, $\overline{N}(\bar{\lambda}, Q, \psi)$, pass through this point and the corresponding value of ultimate buckling load is $\overline{N}_E = (1 - \psi)\overline{N}_L$, where ψ is the erosion factor.

It must be underlined that $\overline{N}_L = Q$ not represents rigorously the theoretical local buckling curve, but it can be assumed (in a simplified way) as a *level* of the cross-section local buckling mode, and,

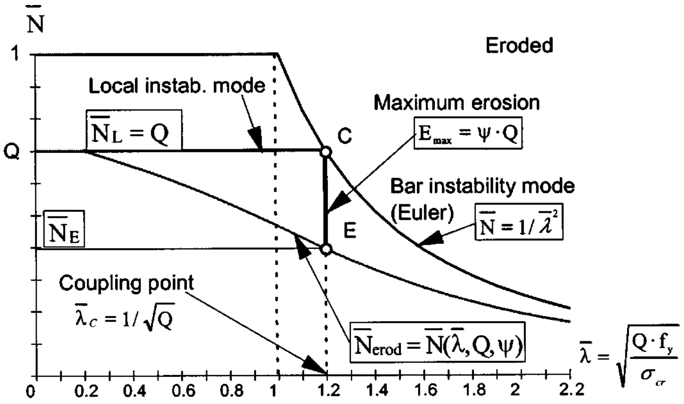

Fig. 5 The interactive buckling model based on the ECBL theory

on the basis of this assumption, it is possibly to evaluate the ultimate strength of the stub column.

3.3. An interpretation of ψ erosion factor in terms of α imperfection coefficient and Q reducing factor of the cross-section area

The solution (5) of the Ayrton-Perry Eq. (4), in the particular point $\overline{\lambda}$=1 has to be taken equal with (1-ψ), because it corresponds to the maximum erosion of the Euler curve when no local buckling occurs (Fig. 6) e.g.,

$$\overline{N}(\overline{\lambda} = 1,\, \alpha) \;=\; \frac{1}{2}[2 + 0.8\alpha - \sqrt{(2 + 0.8\alpha)^2 - 4}] \;=\; 1 - \psi \tag{10}$$

that gives:

$$\alpha \;=\; \frac{\psi^2}{0.8(1-\psi)} \tag{11}$$

or

$$\psi \;=\; 0.4(\sqrt{5\alpha + \alpha^2} - \alpha) \tag{12}$$

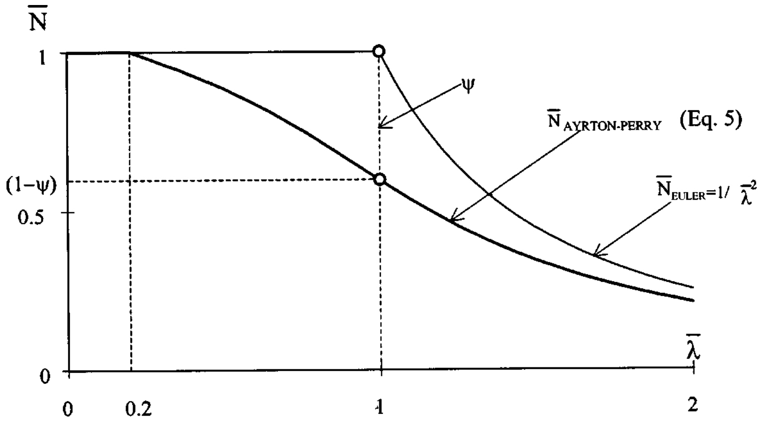

Fig. 6 The erosion of bar buckling curve

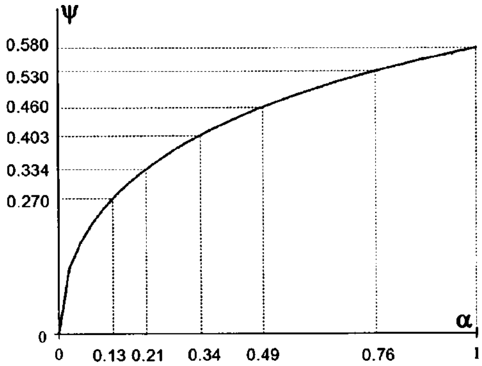

Fig. 7 Relation between ψ erosion factor and α coefficient of imperfection

Fig. 7 shows the change of ψ erosion factor depending on α coefficient of imperfection in European buckling curves.

When local buckling occurs prior to bar buckling, then the solution of Eq. (9), in the coupling point, E (see Fig. 5) is:

$$\bar{N} = \frac{1+\alpha(\bar{\lambda}-0.2)+Q\bar{\lambda}^2}{2\bar{\lambda}^2} - \frac{1}{2\bar{\lambda}^2}\sqrt{[1+\alpha(\bar{\lambda}-0.2)+Q\bar{\lambda}^2]^2-4Q\bar{\lambda}^2} = (1-\psi)Q \tag{13}$$

which leads to

$$\alpha = \frac{\psi^2}{1-\psi}\cdot\frac{\sqrt{Q}}{1-0.2\sqrt{Q}} \tag{14}$$

This represents the new formula of α imperfection coefficient, which should be introduced in European buckling curves in order to adapt these curves to overall-local buckling. Figs. 8 (a and b) show the change of a depending on ψ and Q.

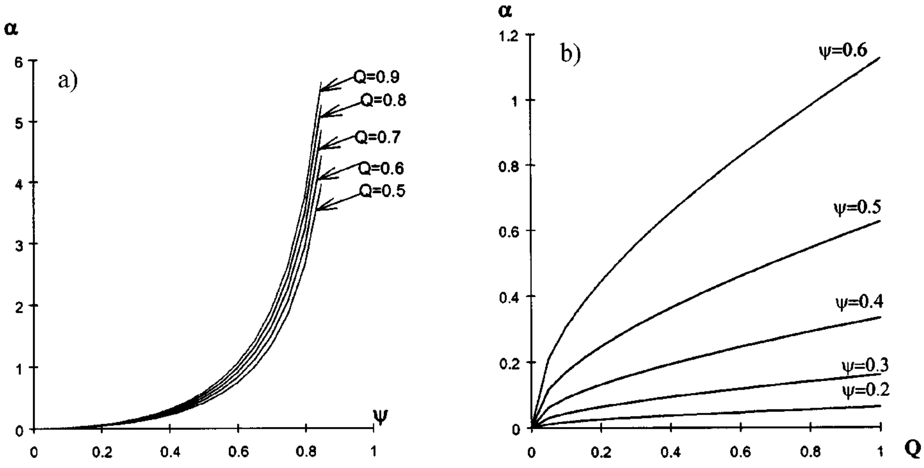

Fig. 8 Relation between α, Q and ψ

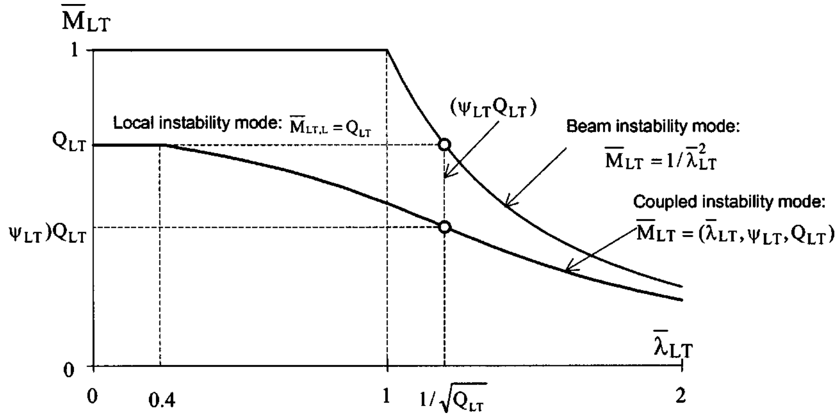

Fig. 9 The ECBL interactive model for thin-walled beams

When one speaks about the erosion of theoretical buckling curve in the coupling point distinction should be made between the *erosion*, expressed by ψ, which refers to the effect of both imperfections and coupling, and the reduced ultimate strength of member, due to local buckling which is introduced by Q factor. An extended discussion of this problem was recently given by Dubina, Ungureanu and Szabo (2000).

3.4. Extension of ECBL interactive approach to thin-walled beams

The previous approach can be very easy extended to the case of interactive local/lateral-torsional buckling of thin-walled beams (Dubina and Ungureanu 1997).

Related to Fig. 9 it can be written for $\bar{\lambda}_{LT} = 1\sqrt{Q_{LT}}$

$$\overline{M}_{LT} = (1 - \psi_{LT})Q_{LT} \tag{15}$$

where

$$\overline{M}_{LT} = \frac{1 + \alpha_{LT}(\bar{\lambda}_{LT} - 0.4) + Q_{LT}\bar{\lambda}_{LT}^2}{2\bar{\lambda}_{LT}^2} - \frac{1}{2\bar{\lambda}_{LT}^2}\sqrt{[1 + \alpha_{LT}(\bar{\lambda}_{LT} - 0.4) + Q_{LT}\bar{\lambda}_{LT}^2]^2 - 4Q_{LT}\bar{\lambda}_{LT}^2} \tag{16}$$

represents the (-) solution of the Ayrton-Perry formula adapted for interactive local-lateral torsional buckling. The generalised imperfection coefficient, in this case, is

$$\eta_{LT} = \alpha_{LT}(\bar{\lambda}_{LT} - 0.4) \tag{17}$$

If $\bar{\lambda}_{LT} = 1/(\sqrt{Q_{LT}})$ is introduced in Eq. (15), after some mathematical processing, this gives:

$$\alpha_{LT} = \frac{\psi_{LT}^2}{1 - \psi_{LT}} \cdot \frac{\sqrt{Q_{LT}}}{1 - 0.4\sqrt{Q_{LT}}} \tag{18}$$

The new ECBL interactive approach for lateral-torsional buckling of thin-walled beams is similar to that of EC 3 -Part 1.3, but instead of ϕ_{LT} given in EC 3 -Part 1.3 the following modified formula should be used:

$$\phi_{LT} = 0.5[1 + \alpha_{LT}(\bar{\lambda}_{LT} - 0.4) + \bar{\lambda}_{LT}^2] \quad (19)$$

with α_{LT} calculated from Eq. (18) in terms of the erosion factor $\psi_{LT.}$

4. Calibration of ψ erosion factor

As evident from previous chapter, in the light of ECBL theory, the key element in the attempt of plotting interactive buckling curves is represented by the erosion coefficient ψ; on this basis the new α imperfection factor, to be used in the European buckling curves, can be evaluated using Eq. (14) and Eq. (18), respectively.

Thus, the necessity of a method to determine the value of coefficient ψ results. In fact, two different methods are possible to this purpose i.e.: experimental and numerical method, respectively.

a) Experimental method

The experimental calibration method requires a relevant set of experimental values located in a close neighbourhood of the coupling point, called "coupling range"

Most often available experimental results scatter, as a result of unavoidable mechanical and geometrical imperfections. Consequently, the concerned specimens do not meet the main requirement of ECBL theory to have a reduced member slenderness identical to the one corresponding to the coupling point ($\bar{\lambda}_C = 1/\sqrt{Q}$, see Fig. 5). Even in case of own specimens, dimensioned with such a length to be *theoretically* located in the coupling point, the imperfections produce an unavoidable scatter of the experimental results and require the work with a coupling range as well.

The selection of the relevant set of specimen should be performed by choosing among *existing results experimental samples reasonably close to the instabilities coupling point* (in terms of reduced slenderness). This is leading to the idea of using a "coupling range", defined in terms of reduced slenderness as a vicinity of the coupling point, instead of working strictly in this point. A correct definition of coupling range limits is therefore of paramount importance for the selection of a relevant set of specimens. Extensive parametric studies (Georgescu 1998) have indicated as acceptable an unsymmetrical coupling range defined around $\bar{\lambda}_c$ with left limit $\bar{\lambda}_1 = 0.85 \cdot \bar{\lambda}_c$ and the right limit $\bar{\lambda}_2 = 1.075 \cdot \bar{\lambda}_c$. All specimens with a reduced slenderness comprised between these two limits should be considered as reasonably close to the coupling point (in terms of reduced slenderness) and selected within relevant experimental set.

b) Numerical method

Based on an advanced non-linear inelastic FEM analysis and taking into account for the imperfections and cold-forming effect, the numerical model has to *simulate* relevant *experimental* values into the *coupling range*.

However, the numerical method, requires also some experimental results in order to calibrate the FEM model.

On the following both experimental and numeric methods will be presented.

4.1. Experimental calibration procedure

Both traditional "mean value" approach or the Eurocode 3 Annex Z one can be used in the experimental method. The first approach was largely shown in several previous publications by author (Dubina *et al.* 1995) and is quite similar to that used in case of numerical calibration, which will be presented into the next chapter. On the following, the EUROCODE Annex Z approach, developed by Georgescu (1998) in his PhD Thesis, will be described.

4.1.1. Eurocode 3 Annex Z based calibration procedure

The calibration procedure, is briefly summarised below in a "step-by-step" manner (Georgescu and Dubina 1999):

STEP 1: Definition of a design model according to EC.3 Annex Z

The following design model is introduced for the theoretical strength function (r_t):

$$r_t = \bar{N} \times A \times f_y \tag{20}$$

with variable $\bar{N}$ defined in relation (13) while A represents the area of gross cross section and f_y the yield stress.

By means of Annex Z procedure, the theoretic strength function r_t should be further calculated using the experimental values of the variables (supposed all available) and compared to the experimentally determined value of the strength r_e.

STEP 2: Checking the conditions for the application of Annex Z procedure

Previous to the application of Annex Z standard procedure, some conditions must be fulfilled i.e.:

- The strength function used to define the design model has to be a product of independent variables;
- Complete sets of measurements are available on all model variables;
- All variables are yielding a log-normal statistic distribution (otherwise Annex Z formulas are not valid).

STEP 3: Application of EC.3 Annex Z standard procedure

By observing relations (13) and (14) it results that strength function value r_t may be easily controlled by modifying erosion factor ψ value. From mathematical point of view $0 < \psi \leq 1$. Practically, erosion factor change is limited to a more narrow range ($0.2 \leq \psi \leq 0.6$) where a series of "k" values for ψ may be defined. Annex Z standard procedure is then applied "k" times per subset, each time with an increased ψ value extracted from the pre-defined series.

Given r_{ti} the values of the design model per specimen i and r_{ei} the values of the strength function determined by experiment, the correction terms are defined for each specimen: $b_i = r_{ei}/r_{ti}$. Their average value called "mean value correction" $\bar{b}$ is also determined. The corrected strength function results, using basic variables average value $\underline{X}_m$:

$$r_m(\underline{X}_m) = \bar{b} \times r_t(\underline{X}_m) = \bar{b} \times (\bar{N}_m \times A_m \times f_{y \cdot m}) \tag{21}$$

Strength characteristic value r_k and strength design value r_d are further determined to Annex Z, followed by safety factor calculation, as terminal point of the procedure: $\gamma_M = r_k/r_d$.

If the required conditions of Annex Z were initially met, the first complete application of the procedure will lead to suitable values of correlation coefficient $\rho > 0.9$, variation coefficient $V_r < 0.15$ and safety factor $\gamma_M < 1.25$, from Annex Z point of view.

As in many cases the experimental values are yielding a considerable scatter, one or even all upper indicators may not comply with the recommended range, which clearly blocks any further use of the procedure.

In this situation the following method is proposed, which has given excellent practical results:

a) Ranging of "b_i" values in increasing or decreasing order (each of the values corresponding to an experimental specimen)

b) Successive elimination of "b_i" values (and corresponding specimens) from the experimental set, starting from one limit of the range, observing the subsequent improvement of concerned statistical indicators *in Annex Z procedure*. The optimum limit of the series (inferior or superior) from where to start the elimination will be detected by attempts.

c) Thus a number of eliminations are performed, until acceptable values for the mentioned indicators are reached. As for the eliminated specimens, two situations are possible:

c.1) Only a small number of specimens have been eliminated from the experimental set, until suitable values for the indicators were reached. In this case the eliminated specimens (of correlation, variation or safety factor reasons) will be further disregarded and considered as out-liers.

c.2) A large or very large number (even majority) of specimens has been eliminated until the remaining sub-set has reached *acceptable values* for the upper statistical indicators. In this case the elimination procedure will be repeated *in the same way as described*, on the large set of eliminated values. A second sub-set of specimen, which fulfils Annex Z, conditions for the indicators will result, together with some eliminated values. If the new eliminated values are still in large number, the procedure will be repeated on them as described. In the end, only a very small number of specimens are actually lost by elimination, but in exchange, the procedure is unblocked and may continue *separately* on the detected sub-sets.

The method proposed (and largely experimented in practical calibrations) by the author (Georgescu 1998) has the advantage of eliminating only an insignificant number of specimens in case of bad correlation, variation or safety factor values, but of detecting a multi-modal structure containing a number of sub-sets on which it is possible to carry on separately the calibration procedure.

STEP 4: Detection of the erosion factor calibrated value ψ_j for each subset *j*

If the values of ρ, V_r, and γ_M obtained from all "*k*" application of Annex Z standard procedure over the concerned sub-set are examined, *only slight changes* of upper factors are observed, produced by the imposed change of ψ erosion factor values. This shows a *low sensitivity* of upper three parameters to the change of the erosion factor ψ.

Thus, no optimisation criterion for ψ may be directly related to ρ, V_r, or γ_M parameters. However, a very strong sensitivity to ψ change has been observed in case of the correction terms b_i.

A *safety range* may be defined by introducing the following obvious requirement for each specimen *i*:

$$\frac{r_{ei}}{r_{ti}} \geq 1 \text{ and } \frac{r_{ei}}{r_{ti}} \leq \gamma_M \tag{22}$$

If the number N_s of the correction terms *included in the safety range* (i.e., $1.0 \leq b_i \leq \gamma_M$) is determined for each application "*k*" of Annex Z standard procedure on concerned subset, a maximum value of this number N_s^{max} will always be found inside ψ variation range. By representing N_s change depending on ψ, a convex curve of the type in Fig. 10 results:

The ψ_j value corresponding to N_s^{max} should be adopted as calibrated value of the erosion factor ψ_j for the statistic mode *j*, corresponding to optimum model behaviour from safety point of view. Thus, the central idea of Annex Z, which establishes the accuracy of a model by evaluating model safety level, is applied.

STEP 5: Obtention of the calibrated value (ψ_c) for the erosion factor

As, up to now, the standard procedure of Annex Z was *separately* applied on each subset of

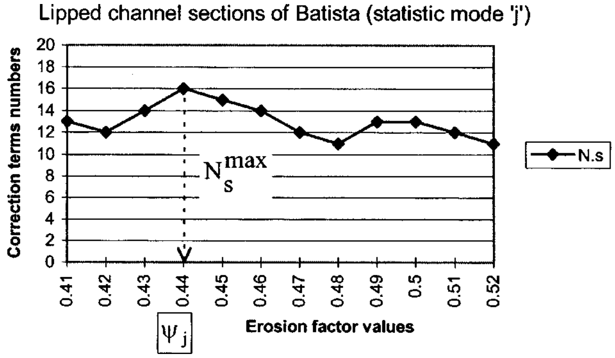

Fig. 10 Change of N_s number depending on ψ factor

experimental values, at the end a number of calibrated values ψ_j will result, corresponding each to one detected sub-set. The authors are proposing to determine the calibrate value ψ_c using the "envelope" principle, so:

$$\psi_c = \max\{\psi_j\} \tag{23}$$

Thus the results of the calibration procedure will always remain on the safe side.

4.1.2. Validation of calibration procedure

The experimental calibration procedure previously presented has been validated using the database with experimental tests on hot-rolled profiles carried out during the European campaign of the years 1960 (Sfintesco 1970).

The aim of this testing procedure was to check if the values of α obtained with the formula (11) are comparable with those initially obtained for the European buckling curves (Rondal and Maquoi 1979). Some of the results obtained by applying proposed procedure are presented in Table 2 and Table 3.

As evident from upper table, the values obtained by calibration are matching at a satisfactory degree the existing framing of profiles cross-sections on the five European buckling curves, which allows for procedure validation.

4.1.3. Results for thin-walled cold-formed compression members

However, the main purpose of the using ECBL approach was to calibrate the imperfection coefficient in case of thin-walled cold-formed profiles, in order to obtain specific buckling curves,

Table 2 Calibrated values of erosion factor (ψ) in case of hot-rolled profiles

Profile type	Statistic mode	Number of specimens	Correlation coef. (ρ)	Variation coef. (V_r)	Safety factor (γ_M)	Erosion coef. (ψ)
IAP-150	1	20	0.817	0.114	1.1834	0.350
	2	24	0.892	0.109	1.1698	0.165
	3	14	0.864	0.108	1.1720	0.334
IPE-160	1	31	0.886	0.124	1.2028	0.330
IPE-200	1	7	0.931	0.115	1.2322	0.280
DIE-200	1	7	0.916	0.115	1.2314	0.410

Table 3 Subsequent (α) values & comparison with the EC3 framing

Profile type	Calibrated (ψ) value	Calibrated (α) value	Resulting buckling curve	EUROCODE 3 framing on curve: (Min. inertia axis)
IAP-150	0.350	0.236	***b***	***b***
IPE-160	0.330	0.203	***a***	***b***
IPE-200	0.280	0.136	***a***	***b***
DIE-200	0.410	0.373	***c***	***c***

Table 4 Calibrated values of the erosion factor (ψ) in case of TWCF profiles

Profile type	Statistic mode	Number of specimens	Correlation coef. (ρ)	Variation coef. (V_r)	Safety factor (γ_M)	Erosion coef. (ψ)
C	1	14	0.965	0.122	1.2577	0.440
	2	12	0.979	0.111	1.2276	0.170
U	1	8	0.882	0.109	1.2568	0.270
□ 300×200×4.98	1	24	0.928	0.099	1.1617	0.370

Table 5 Subsequent (α) values & comparison with the EC3 framing

Profile type	Calibrated (ψ) value	Calibrated (α) value	Resulting buckling curve	EC 3-Part 1.3 framing on curve: (Min. inertia axis)
C	0.440	0.217–0.429	***c***	***b***
U	0.270	0.089–0.125	***a***	***c***
□ 300×200×4.98	0.370	0.233	***b***	***b***

required by their particular stability behaviour.

The proposed calibration procedure has been applied on two sets of experimental values carried out by Batista at the University of Liege/Belgium on "C" and "U" cross-section profiles (Batista 1986), as well as on a set of experimental values on rectangular hollow section extracted from CIDECT database (1992). The obtained results are shown in Table 4 and Table 5.

All calibration results were checked by calculating the percent deviation of the reduced experimental values ($\overline{N}_{exp} = N_{exp}/A \cdot f_y$) in respect with the corresponding ordinate of the resulting buckling curve (see Eq. 24):

$$\Delta\% = \frac{\overline{N}_{exp} - \overline{N}_{curve}}{\overline{N}_{curve}} \cdot 100 \tag{24}$$

The computed results may be put in form of histograms, which the position of the experimental points in respect with the relevant buckling curve like shown in Fig. 11.

By examining the upper histogram, a strong scatter of the experimental values is visible, but also the fact that the calibration result is situated on the safe side, which evidently confirms it.

4.2. Numerical calibration procedure

4.2.1. Calibration of advanced analysis FEM model (Dubina et al. 1997)

Very accurate tests performed at University of Sydney on compressed cold-formed "C" sections

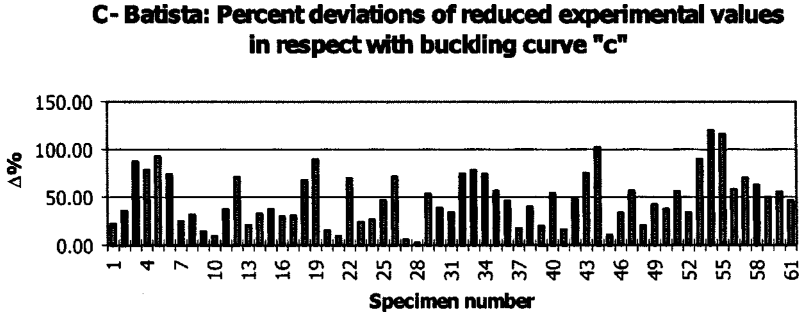

Fig. 11 Percent deviations of the experimental values in respect with the buckling curve

Table 6 Measured specimen dimensions for series L36 (Young and Rasmunssen 1995)

Specimen	Lips B_l (mm)	Flanges B_f (mm)	Web B_w (mm)	Thickness t (mm)	Thickness t^* (mm)	Radius r_i (mm)	Length L (mm)
L36P0280–	12.6	37.1	97.2	1.53	1.48	0.85	279.9
L36P0815+	12.7	37.0	97.4	1.51	1.48	0.85	814.6
L36P1315–	12.4	36.9	97.1	1.52	1.47	0.85	1316.4

(Young and Rasmunssen 1995) were used as basis of the calibration of numerical model. The nominal cross-section dimensions for the series specimen are: thickness of 1.5 mm, web width of 96 mm, flange width of 36 mm and lip width of 12 mm. The lipped channels were brake-pressed from zinc-coated structural steel sheets Grade G 450 of (nominal yield stress of 450 MPa). Table 6 shows the measured dimensions of the specimens.

Material properties, determined from coupon tests, are: 0.2% tensile proof stresses ($\sigma_{0.2}$) of 500 MPa, tensile strength (σ_u) of 540 MPa and Young's modulus $E = 195$ GPA. In Table 6, t^* represents the metal thickness and it was used in FEM model, together with measured cross-section dimensions and determined material properties.

The dimension of the pin-ended bearing (95 mm at each end) should be added to the pin-ended specimen length for the pin-ended columns. The pinned end bearings allow for rotation about the minor y-axis, only.

4.2.1.1. Introduction of geometrical imperfections and material non-linearities

From the point of view of non-linear analysis, initial imperfections are used in order to lead the load-displacement response of model to certain instability shape. In case of compressed members some kind of disturbance is essential because loading itself has no distorting effect on the model. When initial imperfection is used to invoke geometric non-linearity, the shape of imperfection can be determined with eigen buckling analysis. The eigen buckling modes should describe the possible displacement field for the member.

Two kind of geometric imperfections were taken into account in FEM model: overall geometric imperfection (with maximum size, f_o, at the mid-length), and local web imperfection of w_o amplitude. The geometric imperfections used into the FEM model were taken as follows:

–for L36280 - and L36P815+ specimens, the local imperfection is affine with the first local buckling mode, and the overall imperfection is taken as a single wave-length sine shape of f_o amplitude;

–for L36P1315 - specimen, the overall imperfection is affine with the first buckling mode, (flexural buckling) while the local imperfection is affine with the second buckling mode (local buckling).

The size of imperfections was equal either with the measured or equivalent overall and local initial deflections. The measured amplitude of local imperfections is the maximum out-of-plane deflection, measured at the middle of the web width, while the overall one is the initial deflection at mid-length of the member.

Equivalent overall amplitude was taken (l/1000) of column length, according to EUROCODE 3-Part 1 provisions; the local equivalent imperfection was 0.006 of web width (Schafer and Pekoz 1996). The measured eccentricity (e_o) of the applied load, was also introduced in FEM model.

The membrane and the flexural measured residual stresses had values from 15 MPa to 40 MPa. As pointed out for the authors of the tests, the residual stresses, compared with the nominal yield stress, which is 450 MPa are negligible, and, consequently they were not introduced in the FEM model.

The material behaviour was introduced using the ideally elastic-plastic bilinear model (Prandtl) and a non-linear one, based on the Ramberg-Osgood formula calibrated for the considered material ($\sigma_{0.2}$=500 MPa, σ_u=540 MPa, ε_u=12%).

4.2.1.2. FEM procedure

The numerical analysis was carried out with ANSYS 5.3 using SHELL 43 elements. This is a 4 node element, allowing for elastic-plastic large strains and deflection analysis. Boundary conditions and loading are set to match those employed in the physical tests.

4.2.1.3. Numerical results

Numerical results obtained with ANSYS large-deformation elastic-plastic analysis are presented in Table 7.

4.2.2. Calibration of ψ erosion factor

In this paragraph the calibration of ψ erosion factor via numerical procedure is presented. For this purpose, the *mean value* statistical procedure was used. This procedure includes the following steps:

Table 7 Ultimate loads in kN

Specimen	Tests	ANSYS with bilinear material model		ANSYS with R-O model
		Measured imperfections	Equivalent imperfections	Measured imperfections
L36P0280–	83.5	–	85.87	81.41
L36P0815+	67.9	70.5	72.08	69.8
L36P1315–	41.1	41.42	38.56	40.75

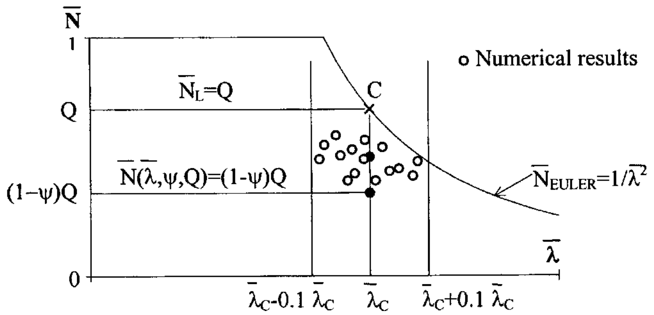

Fig. 12 Evaluation of ψ erosion factor by means of numerical results

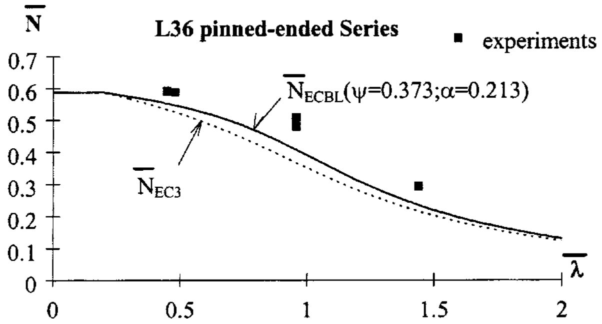

Fig. 13 Theoretical/experimental comparative results

1. Evaluation of ultimate load of member in the coupling point which is defined by the interactive slenderness, $\bar{\lambda}_C = 1/\sqrt{Q}$, and also at the limit points of the coupling range, considered to be symmetrical, $\bar{\lambda}_C \pm 0.1 \cdot \bar{\lambda}_C$ (Fig. 12).

Two different ultimate loads corresponding to $\pm f_o$ amplitude of overall geometrical imperfection, will be calculate in each point. The local imperfections, w_o, is the same in all cases.

2. Compute the individual value of erosion, $\psi_i = Q_i - \frac{N_{i,\,num}}{N_{i,\,pl}}$, for the i specimen, and the mean value of the erosion factor, $\psi_m = \frac{1}{n}\sum_{i=1}^{n} \psi_i$, for all n members.

3. Compute the *design value* of the erosion factor:

$$\psi_d = \psi_m + 1.64s \tag{25}$$

where s is the standard deviation which is introduced in order to take into account the randomness of numerical results.

4.2.3. Numerical results

The numerical approach was used to obtain the erosion value corresponding to the L36 specimen series (Young and Rasmunssen 1995). The length corresponding to $\bar{\lambda}_C$ was 1304 mm (including the pin-ended bearings).

With f_o=±0.46 mm and w_o = 0.25 mm, ANSYS large-deformations elastic-plastic (bilinear material model) analysis has given an erosion of $\psi = 0.373$, and, after the a imperfection factor resulted equal to 0.213.

Fig. 13 shows the comparison between the experimental values with the Eurocode 3-Part 1.3 buckling curve and the buckling curve obtained with the numerically calibrated value of ψ (both numerical and code curves were divided by γ_{M1}=1.1 safety coefficient). The agreement between experimental values and the numerical buckling curve is satisfactory.

5. Elastic-plastic interactive buckling formula via ECBL approach

As shown in Chapter 2 of this paper, due to the localisation of buckling patterns, the localised post-buckling of stub column leads always to a local plastic mechanism mode of failure. This fact is

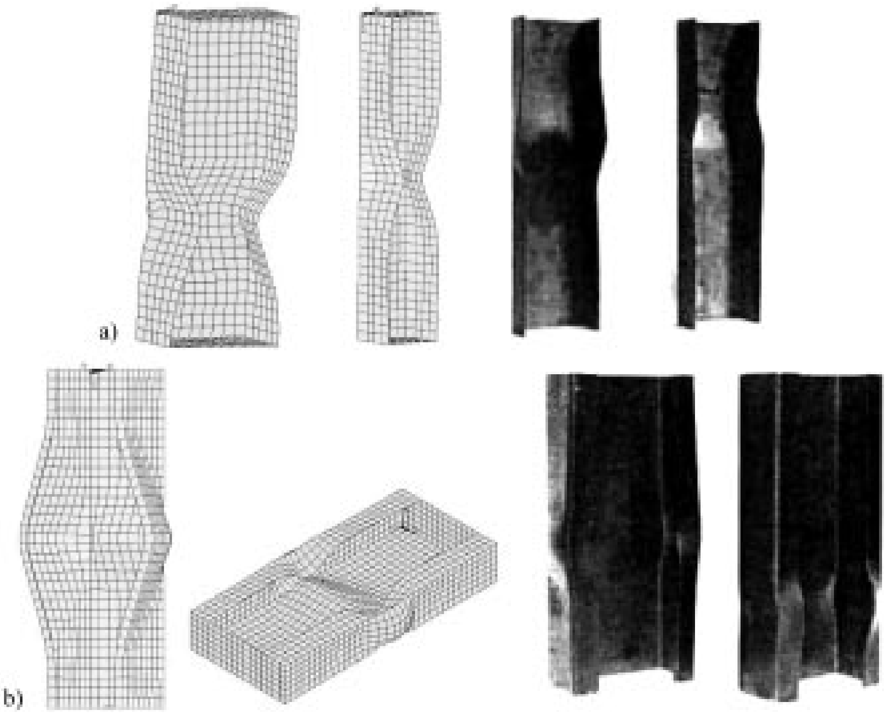

Fig. 14 Plastic mechanisms of plain and lipped channel stub columns: tests and FEM simulation

confirmed both by tests and numerical simulations (Fig. 14).

Starting from this real behaviour of thin-walled stub columns, and based on the Murray theory (Murray and Khoo 1981), Dubina and Ungureanu (2000) used the ECBL approach in order to express the plastic-elastic interactive buckling of thin-walled compression members.

In this case the *erosion* can be associated to the plastic-elastic interaction between the *rigid plastic mode* (plastic strength) of stub column and the overall elastic buckling mode of the bar, given by Euler formula.

The main problems of this approach is to evaluate properly the plastic strength of thin-walled stub column, via the local plastic mechanism theory, and after the erosion of critical load into the "*plastic-elastic coupling range*".

Fig. 15 shows the ECBL approach adapted to plastic-elastic interactive buckling.
where:

N_U = ultimate compression strength;
N_{pl} = $A \times f_y$ full plastic strength of thin-walled cold-formed members;
$N_{pl,m}$ = the local plastic buckling (mechanism) strength;
A = the gross area of cross section;
$\overline{\lambda}$ = relative slenderness in overall buckling;
$\overline{\lambda}_C$ = relative slenderness in the coupling point.

Following exactly the same way as for the elastic local-overall interactive buckling, the α imperfection factor for the plastic-elastic interactive buckling results:

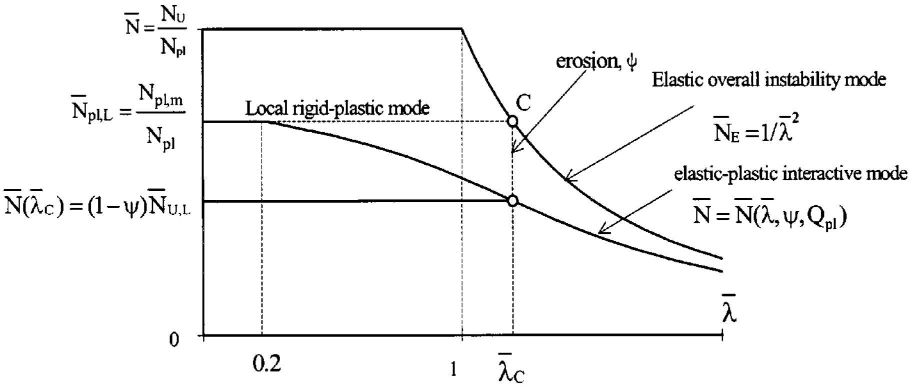

Fig. 15 The interactive buckling model based on the ECBL theory

$$\alpha = \frac{\psi^2}{1-\psi} \cdot \frac{\sqrt{Q_{pl}}}{1-0.2\sqrt{Q_{pl}}} \tag{26}$$

where Q_{PL} is the reduction factor of plastic strength of this member,

$$Q_{pl} = \overline{N}_{pl,L} = \frac{N_{pl,m}}{A \cdot f_y} \tag{27}$$

In order to evaluate the ψ erosion factor, the “mean value” experimental approach was used.

The same experimental data carried out at the University of Liege (Batista 1986) were used to compare the ECBL plastic-elastic approach with the elastic-elastic one, and with Eurocode3 - Part. 1.3 and advanced FEM results.

The experimental procedure with the “mean value” statistical approach, considering the coupling range to be $\overline{\lambda} \pm \varepsilon = 1/\sqrt{Q_{pl}} \pm 0.20$ was used in order to provide the numerical results for this comparison.

The experimental “mean value” approach includes the following steps:

1. Compute the *individual* erosion for the i column specimen

$$\psi_i = \overline{N}_{pl,L} - \overline{N}_{i,exp} \tag{28}$$

where

$$\overline{N}_{i,exp} = \frac{\overline{N}_{i,exp}}{\overline{N}_{i,pl}} \tag{29}$$

with $N_{i,exp}$, the experimental failure load and $N_{i,pl}=A_i \times f_y$ the full plastic resistance of the i specimen.

2. Compute the mean value of ψ erosion factor for all n specimens, with the same cross-section shape, included into the coupling range:

$$\psi_m = \frac{1}{n}\sum_{i=1}^{n}(\overline{N}_{pl,L} - \overline{N}_{i,exp}) \tag{30}$$

3. Compute the *design* value of the erosion factor:

$$\psi_d = \psi_m + 1.64s \tag{31}$$

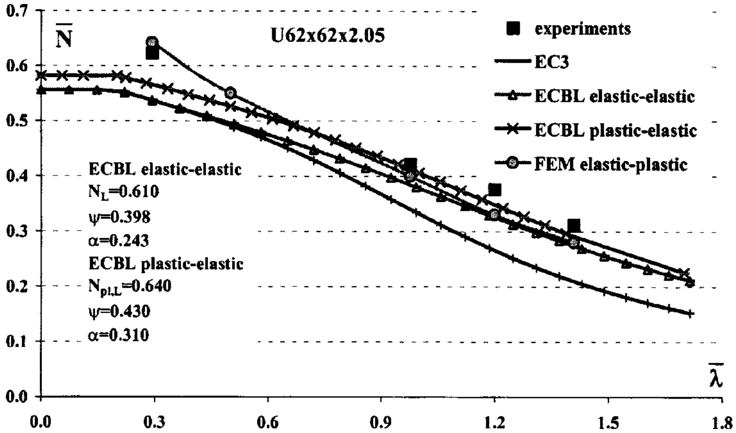

Fig. 16 Numerical/Experimental comparison for plain channel sections subject to compression tested by Batista (1986)

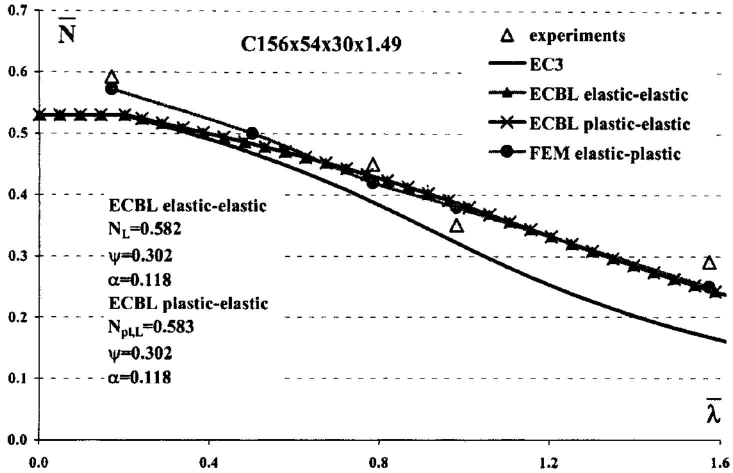

Fig. 17 Numerical/Experimental comparison for lipped channel sections subject to compression tested by Batista (1986)

in which s is the standard deviation related to ψ_i and ψ_m values.

Figs. 16 and 17 show the comparative results for plain and for lipped channels, respectively. According to Eurocode 3 Part. 1.3, the safety factor γ_{M1}=1.1 was used for all numerical results.

6. Conclusions

Coupled instabilities represent a characteristic of thin-walled steel members in compression. Actual buckling curves of design codes, in Europe for instance, are based on experimental tests carried out on hot-rolled sections. On the purpose of practical use these curves have been adapted in order to cover the stability design problems of thin-walled cold-formed steel sections.

However, compared to hot-rolled ones, these sections have different properties which refer to their geometry, cold-formed effect, residual stresses, influence of geometrical imperfections and, very important, to the phenomenon of coupled instability.

All these reasons lead to the necessity of specialised buckling curves for thin-walled cold-formed steel sections. At present, it would be difficult to organise and support an experimental campaign, similar to that realised in 60's in Europe to establish buckling curves for hot-rolled sections. Therefore, the variety of shapes of thin-walled cold-formed steel sections make a such campaign impossible.

The ECBL approach seems to be a practical and convenient tool to continuously adapt the existing buckling curves for thin-walled cold-formed steel sections.

On this purpose, a limited number of tests are necessary, only. Using of numerical simulations is also possibly.

Both members in compression and bending can be analysed. Local plastic-overall elastic interactive buckling can be also represented.

Very important too, the theoretical background of ECBL approach, based on the erosion theory of coupled bifurcation, is much more rigorous and understandable than the semi-empirical methods used for the buckling curves in existing design codes.

References

Al-Bermani, F.G.A. *et al*. (1994), "Stability of cold-formed members", *Engng. Struct.* **16**, 386-392.

Batista, E (1986), "Essais de profils C et U en acier plies a froid", *Raport* **N^o 157**, Universite de Liege, Laboratoire de Stabilite des Constructions.

CIDECT Report (1992), "Inventory of the research on hollow sections carried out in the stability field", Part two Databank of CIDECT Experimental Tests, **2M-92/2**.

Dubina, D. (1990), "A new approach to the interaction of local and overall buckling in thin-walled cold-formed compressed members - final report", *Proceedings of 4th Int. Coll. on Stability of Steel Structures*, Budapest, April 25-27, 412-419.

Dubina, D. (1993), "Coupled instabilities in thin-walled structures: Erosion coefficient approach in overall-local buckling interaction", *Commission of the European Communities*, Cooperation in Science and Technology with Central and Eastern European Countries Research Report, Ref. ERB 3510PL922443, Liège.

Dubina, D. *et al.* (1995), "Calibration of interactive buckling erosion factor via a cold-formed steel sections experimental data base", *Int. Coll. on Stability of Steel Structures*, Hungary, Budapest, September 21-23, II, 133-144.

Dubina, D. (1996), "Coupled instabilities in bar members-General Report", *Proceedings of 2nd Int. Conf. on Coupled Instabilities in Metal Structures CIMS96*, Liege, September 5-7, 119-132.

Dubina, D. and Ungureanu, V. (1997), "Lateral-torsional and local interactive buckling of thin-walled cold-formed beams", *Revue Roumain des Sciences Techniques, Mécanique Aplliquée*, **42**(5-6), 467-481.

Dubina, D. *et al.* (1997), "Numerical modelling of instability phenomena of thin-walled steel members", *Proceedings of 5th International Colloquium on Stability and Ductility of Steel Structures - SDSS97*, Nagoya, Japan, July 29-31, **2**, 755-767.

Dubina, D. (1998), *Part. VI: Interactive Buckling Analysis of Thin-walled Cold-formed Steel Members via Critical Load Erosion Theory in Coupled Instabilities in Metal Structures*, Edited by J. Rondal, Springer-Verlag, 291-344.

Dubina, D. and Ungureanu, V. (2000), "Elastic-plastic interactive buckling of thin-walled steel members", *Structural Stability Research Council Annual Technical & Meeting*, July 24-26, Memphis, USA.

Dubina, D., Ungureanu, V. and Szabo, I. (2000), "Influence of local and sectional geometrical imperfections on the local/distortional and interactive buckling modes of cold-formed members", *Proceedings of 3rd Int. Conf. on Coupled Instabilities in Metal Structures*, September 14-16, Lisbon, Portugal.

EUROCODE 3 (1996), *Design of Steel Structures. Part 1.3: General rules. Supplementary Rules for Cold-*

Formed Thin Gauge Members and Sheeting, ENV 1993-1-3, February.

Georgescu, M. (1998), “Instability problems by thin-walled cold-formed steel members”, PhD Thesis, The Politehnica University of Timisoara.

Georgescu, M. and Dubina, D. (1999), “E.C.B.L. and EUROCODE 3 Annex Z based calibration procedure for buckling curves of compression steel members”, *Proceedings of 6th International Colloquium on Stability and Ductility of Steel Structures - SDSS'99*, Timisoara, September 9-11, 501-510.

Gioncu, V. *et al*. (1992), “Coupled instabilities in mono-symmetrical steel compression members”, *J. Construct. Steel Research*, **21**, 71-95.

Gioncu, V. (1994), “General theory of coupled instabilities”, *Thin-Walled Structures*, **19**(2-4), 81-127.

Hancock, G.J. *et al*. (1994), “Strength design curves for thin-walled sections undergoing distortional buckling”, *J. Construct. Steel Research* **31**, 169-186.

Lau, S.C.W. and Hancock, G.J. (1988), “Strength tests and design methods for cold-formed channel columns undergoing distortional buckling”, Research Report **R579**, School of Civil and Mining Engineering, University of Sydney, Australia.

Lau, S.C.W. and Hancock, G. (1990), “Inelastic buckling of channel columns in the distortional mode”, *Thin-Walled Structures* **10**(1990), 59-84.

Menken, G.M. *et al.* (1991), “Interactive buckling of beams in bending”, *Thin-Walled Structures* **12**(1991), 415-434.

Murray, N.W. and Khoo, P.S. (1981), “Some basic plastic mechanisms in the local buckling of thinwalled steel structures”, *Int. J. Mech. Sci.*, **23**(12), 703-713.

Rondal, J. and Maquoi, R. (1979), “Formulation d’Ayrton-Perry pour le flambement des barres métalliques”, *Construction Métallique*, **4**(1979), 41-53.

Schafer, B. and Pekoz, T. (1996), “Geometric imperfections and residual stresses members”, *Thirteenth International Speciality Conference on Cold-Formed Steel Structures*, St. Louis, Missouri, USA, October 17-18, 649-664.

Sfintesco, D. (1970), “Fondement experimental des curbes europeenes de flambement”, *Construction Métallique*, **3**(1970).

Young, B. and Rasmunssen, K.J.R. (1995), “Compression tests of fixed-ended and pin-ended cold-formed lipped channels”, Research Report R715, School of Civil and Mining Engineering, University of Sydney, Australia.